BIOCHEMISTRY
including biophysical chemistry & molecular biology

Article

pubs.acs.org/biochemistry

Identification of Minimal HDV-Like Ribozymes with Unique Divalent Metal Ion Dependence in the Human Microbiome

Nathan J. Riccitelli,[†] Eric Delwart,[‡,§] and Andrej Lupták*[,†,∥,⊥]

[†]Department of Chemistry, [∥]Department of Pharmaceutical Sciences, and [⊥]Department of Molecular Biology and Biochemistry, University of California—Irvine, Irvine, California 92697, United States

[‡]Blood Systems Research Institute, 270 Masonic Ave, San Francisco, California 94118, United States

[§]Department of Laboratory Medicine, University of California—San Francisco, San Francisco, California 94143, United States

Supporting Information

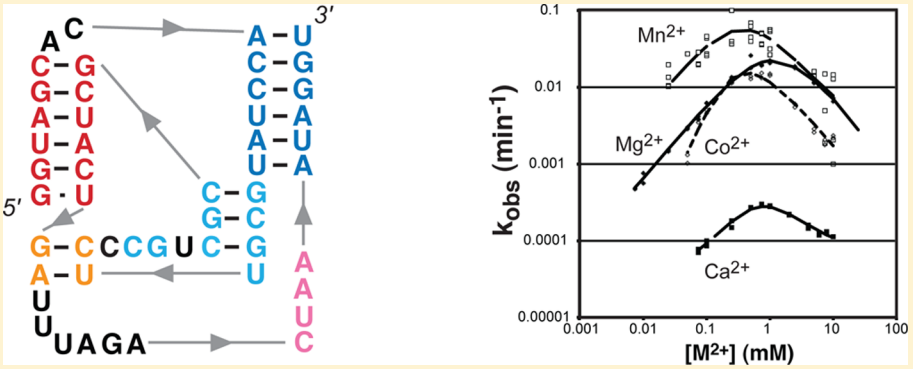

ABSTRACT: HDV-like self-cleaving ribozymes have been found in a wide variety of organisms, implicated in diverse biological processes, and their activity typically shows a strong divalent metal dependence, but little metal specificity. Recent studies suggested that very short variants of these ribozymes exist in nature, but their distribution and biochemical properties have not been established. To map out the distribution of small HDV-like ribozymes, the drz-Spur-3 sequence was minimized to yield a core construct for structure-based bioinformatic searches. These searches revealed several microbial ribozymes, particularly in the human microbiome. Kinetic profile of the smallest ribozyme revealed two distinct metal binding sites, only one of which promotes fast catalysis. Furthermore, this ribozyme showed markedly reduced activity in Ca^{2+}, even in the presence of physiological Mg^{2+} concentrations. Our study substantially expands the number of microbial HDV-like ribozymes and provides an example of cleavage regulation by divalent metals.

The HDV ribozymes are among several RNAs that fold into structures promoting scission of their own backbone.[1] This activity occurs through 2′OH attack on the phosphate group of the adjacent nucleotide, producing a 2′-3′ cyclic phosphate and 5′ hydroxyl. Despite this common mechanism of self-scission, the secondary structures for the various classes of ribozymes are diverse.

The structure of the HDV ribozymes consists of five helical domains (P1, P2, P3, P1.1, and P4) arranged into a nested double-pseudoknot, with P1, P1.1, and P4 forming one coaxially stacked helix, and P2 and P3 forming another. Short single-stranded regions link the base-paired domains. The active site of the ribozyme is built around the L3, P1.1, and J4/2 regions, with the J4/2 containing the catalytic cytosine residue that acts as the proton donor in the cleavage reaction.[2−8] The genomic and anti-genomic HDV ribozymes require a divalent metal ion for full catalytic activity, and the activity-pH profile is flat over a wide pH range, suggestive of two active-site titratable groups, one of which likely corresponds to the catalytic cytosine nucleobase.[5,6,9−11]

Several other nucleotides in the ribozyme core form crucial interactions that promote catalysis. In the genomic HDV ribozyme, the U20 and G25 residues at the base of the P3 helix form a reverse G•U wobble pair that positions the N7 and O6 atoms of the guanine base to bind the catalytic metal.[5] The G25 stacks on the conserved C24 residue, which in turn forms a hydrogen bond with the pro-S_p phosphate of C22 and creates a niche centered on the active site.[2,4,5] In the J4/2 region, a conserved adenosine residue forms an A-minor interaction with the C18-G29 base-pair of the P3 helix and helps position the catalytic C75 residue into the cleavage site.[2] Finally, the pro-R_p oxygen of the scissile phosphate contacts the catalytic metal, and in one genomic ribozyme crystal structure, it forms a sharp U-turn kink that promotes release of the upstream product following scission.[5,12,13] The identity of this nucleotide has a

Received: December 28, 2013
Revised: February 17, 2014
Published: February 20, 2014

dx.doi.org/10.1021/bi401717w | *Biochemistry* 2014, 53, 1616−1626

marked effect on catalysis and possibly facilitates the binding of a second metal ion that reduces the overall catalytic rate.[12,14,15]

Since their initial discovery in the HDV genome, HDV-like ribozymes have been found in many species, mostly in genomes of multicellular eukaryotes, through *in vitro* selections and structure-based bioinformatic searches.[16−18] One of these ribozymes, the sea urchin drz-Spur-3 sequence, contained a shortened, 6 base-pair P1 helix, yet exhibited robust self-scission under physiological-like conditions (k_{obs} = 0.2 min^{-1} at 1 mM Mg^{2+}, 22 °C).[16] Previous mutagenesis of the genomic and anti-genomic HDV ribozymes demonstrated their tolerance to deletions in the P4 helix, but variations in the P1 helix length have not been examined.[19−21] Indeed, the structure-descriptor used to find the drz-Spur-3 sequence specified a seven base-pair P1 helix, and subsequent analysis of the upstream cleavage product revealed that this ribozyme contained a shortened P1 region.[16] The drz-Spur-3 ribozyme thus represented the first naturally occurring instance of a six base-pair P1 helix, suggesting that the structure descriptors used in initial searches for HDV-like ribozymes were too restrictive in their requirements and likely overlooked additional, smaller HDV-like self-cleaving sequences.

To further explore the distribution of small HDV-like ribozymes in genomic space, we set out to determine the minimum secondary structure required for self-scission. Using the minimal motif, we defined secondary-structure descriptors that searched available genomes and metagenomic sequence data for HDV-like ribozymes possessing shortened P1, P2, J1/2, and J1.1/4 regions, and no P4 helix. This search yielded a number of putative ribozymes in a wide range of species, but unlike the larger HDV-like ribozymes, these minimal examples we predominantly found in bacteria. Of particular note was a group of highly similar ribozymes found in a microbial metagenomic data set derived from sewage samples.[22] One of the these ribozymes showed a distinct, bell-shaped divalent metal ion dependence, irrespective of the identity of the nucleotide at the −1 position, suggesting the presence of a secondary metal binding site that alters the catalytic metal binding pocket. In addition, this ribozyme showed a markedly slow activity in Ca^{2+}, which also noncompetitively inhibits Mg^{2+}-dependent reaction. Our study shows that the HDV-like family of ribozymes extends to microbial genomes, where it consists primarily of sequences near the lower length-limit of the double-pseudo-knot secondary structure characteristic of these ribozymes.

EXPERIMENTAL PROCEDURES

1. Secondary Structure-Based Searches. The RNABOB program (courtesy of S. Eddy, HHMI; ftp://selab.janelia.org/pub/software/rnabob/) was used to define the conserved sequence and structure elements for minimal HDV-like ribozymes based on the drz-Spur-3-min sequence. The descriptor used for the searches is provided below. For further information regarding the RNABOB descriptor format and usage, see ref 24.

```
h1 s1 h2 r3 s2 h4 s3 r3′ h1′ h4′ s5 s6 h2′ s7
h1 0:0 GNNNNN*:*NNNNNY
s1 0 N[50]
h2 0:1 ***NNNNNN:NNNNNN***
r3 0:0 NNN:NNN TGCA
s2 0 T
h4 0:0 YC:GN
s3 0 NCG*Y
s5 0 NNNN[15]
s6 0 CNRA
s7 0 NNNNNNNNNNNNNNNNNNNNNNNNN
```

2. DNA Template Preparation. Constructs were prepared by mutual priming of the two synthetic, PAGE-purified oligonucleotides obtained from Invitrogen custom DNA synthesis or IDT. For each ribozyme, one of these oligos was termed the "forward" strand and contains a T7 promoter, a GGGAG transcription start site, ∼20 nucleotides of the genomic sequence upstream of the ribozyme cleavage site, and several nucleotides of the ribozyme, while a second oligo, termed "reverse" strand, contains the reverse complement of the entire ribozyme sequence as well as several nucleotides downstream of the ribozyme. Drz-Spur-3 mutants were constructed using appropriate variants of the drz-Spur-3 WT oligos (SI Table 1). Each construct also used an inhibitor that consisted of nucleotides complementary to a region spanning the cleavage junction. All oligos are listed in the 5′ to 3′ orientation.

Primer extension was carried out in a 100 μL volume containing, at [final], 1X of DreamTaq 2X PCR master mix (Thermo Scientific cat) and 5 μM of each synthetic oligo. Following primer extension, 1 μL of the unpurified primer extension reaction was added to a 100 μL PCR reaction containing 1X of DreamTaq 2X PCR master mix (Thermo Scientific), 10 μM forward PCR primer, 10 μM reverse PCR primer, and water to volume, subjected to 2 cycles of PCR, and stored at −20 °C prior to use in transcription reactions.

3. RNA Transcription. ^{32}P body-labeled RNA was transcribed at 37 °C for one hour in a 20 μL containing 40 mM of tris-HCl (Sigma), 0.01% triton X-100 (Sigma), 2 mM spermidine (Sigma), 30 mM DTT (Sigma), 2.5 mM each GTP, UTP, and CTP, 250 μM ATP, 1.25 μCi [α-^{32}P]-ATP (Perkin-Elmer, Waltham, MA), 7.75 mM $MgCl_2$ (Sigma), 20 μM of a DNA inhibitor oligo (specific for each construct, IDT), 1 unit of T7 RNA polymerase (courtesy of K. Pobanz), and 0.50 pmol of DNA template. The inhibitor oligos were designed to span the RNA cleavage junction of a particular construct with an approximate melting temperature of 50 °C in order to reduce the amount of cotranscriptional cleavage. Unlabeled RNA transcriptions were similar in composition, differing only in their lack of radioactive ATP, and presence of equal concentrations (2.5 mM) of each nucleotide, with equivalent increase in Mg^{2+}.

PAGE purification of RNA began with addition of equal volume of stop/gel-loading buffer (7 M urea, 0.01% SDS, 40 mM EDTA, and bromophenol blue to color) to the transcription reaction prior to loading onto a 7.5% denaturing polyacrylamide gel. Gels were exposed on a phosphorimage screen (GE Life Sciences) and analyzed using the Typhoon phosphorimager (GE Life Sciences) following electrophoresis. Bands corresponding to the uncleaved ribozymes were cut out and the RNA eluted from them in 100 μL of ddH_2O for 1 h. After elution, the solution was spun at 4000 rpm for 5 min through Sephadex G-25 beads (Sigma) to remove small molecules, and frozen at −80 °C.

4. Self-Cleavage Kinetics. In a typical kinetic reaction, purified ^{32}P-labeled RNA solutions were warmed to room temperature, then 1/10th of the final kinetic reaction volume of RNA was added to the kinetic reaction buffer (140 mM KCl, 10 mM NaCl, and 50 mM Tris-HCl, pH 7.4) incubating at the desired temperature (25 or 37 °C) and allowed to equilibrate for five minutes. Self-scission was initiated by addition of a

dx.doi.org/10.1021/bi401717w | *Biochemistry* 2014, 53, 1616−1626

divalent metal at the concentrations tested. At various time points, a small aliquot of the kinetic reaction mixture was taken and mixed with an equal volume of stop/gel-loading buffer. Each time point was resolved by 7.5% denaturing PAGE followed by exposure on a phosphorimage screen and subsequent radiographic analysis using the ImageQuant software package.

During pH analysis, the a kinetic reaction was performed as described above, but with the pH of the kinetic reaction buffer lowered (~4.5−7.5) using a 25 mM MES, 25 mM acetic acid, 50 mM tris base solution or raised (~7.5−9.5) using a 50 mM MES, 25 mM tris base, 25 mM 2-amino-2-methyl-1-pentanol solution.

5. Data Fitting. Self-cleavage data was fit to either the mono- or biexponential decay function:

$$k_{obs} = A \bullet e^{(-k_1 t)} + C \quad (1)$$

or

$$k_{obs} = A \bullet e^{(-k_1 t)} + B \bullet e^{(-k_2 t)} + C \quad (2)$$

where A, B, and C represent the relative fraction of the ribozyme population cleaving at rate k_1, k_2, or remain uncleaved, respectively. When self-cleavage kinetics used biexponential fits, only the fast rate was reported for rate−metal or rate−pH analysis.

Rate−metal plots for ribozymes not exhibiting a decrease in catalysis at elevated metal concentrations were fit to a model assuming only a single binding event that results in self-scission at rate k_1:

$$(3)\quad \mathbf{Rz + M1} \overset{K_{d1}}{\rightleftharpoons} \mathbf{[Rz{\bullet}M1]} \downarrow k_1$$

This yields a rate−metal relationship, allowing for the Hill coefficient (n), of

$$k_{obs} = \frac{k_{max}}{1 + \left(\frac{K_d}{[Mg^{2+}]}\right)^n} \quad (4)$$

For the drz-Mtgn-1 ribozyme, which displays a bell-shaped activity−metal relationship, a dual metal binding/mode was used. This method assumes the existence of at least two ribozyme conformations, which may or may not be catalytically active states, and the presence of these states are modulated by levels of divalent metals in solution:

$$(5)\quad \mathbf{Rz + M1} \overset{K_{d1}}{\rightleftharpoons} \mathbf{[Rz{\bullet}M1] + M2} \overset{K_{d2}}{\rightleftharpoons} \mathbf{[Rz{\bullet}M1{+}{\bullet}M2]} \quad \downarrow k_1 \qquad \downarrow k_2$$

Yielding a rate−metal relationship, allowing for a Hill coefficient in the first channel only, of

$$k_{obs} = k_1 \cdot \left(\frac{(^1[Mg^{2+}])^n}{\frac{(K_{d1})^n}{Q}} \right) + k_2 \cdot \left(\frac{(^1[Mg^{2+}])^n \cdot {}^2[Mg^{2+}]}{\frac{(K_{d1})^n \cdot (K_{d2})}{Q}} \right) + k_3 \cdot \left(\frac{1}{Q} \right) \quad (6)$$

In most cases, n = 1, except for drz-Mtgn-1 in cobalt chloride, where the apparent Hill was 1.9 for the first mode of binding. The third channel, or binding mode accounts for the residual activity we observed when incubating drz-Mtgn-1 RNA in physiological kinetics buffer. This could be due to monovalent-promoted self-scission, or residual Mg^{2+} from transcription, although stringent EDTA treatment (~20 mM, with 7 M urea) prior to transcription purification is designed to minimize the latter.

Q, the partition coefficient, represents the sum total of ribozyme states. From eq 5, this can be defined as

$$Q = 1 + \frac{(^1[Mg^{2+}])^n}{(K_{d1})^n} + \frac{(^1[Mg^{2+}])^n \cdot {}^2[Mg^{2+}]}{(K_{d1})^n \cdot K_{d2}} \quad (7)$$

For activity-pH profiles, two titratable groups, the catalytic cytosine (pK_{a1}) and a hydrated metal ion (pK_{a2}), in these experiments always Mg^{2+}, were assumed present, leading to an equation of

$$k_{obs} = \frac{k_{max}}{1 + 10^{pH - pKa_1} + 10^{pKa_2 - pH} + 10^{pKa_2 - pKa_1}} \quad (8)$$

6. Phosphorothioate Interference Mapping. The drz-Mtgn-1 DNA was transcribed in conditions similar to the nonradioactive transcriptions described above for 45 min (approximately the half-life of the ribozyme in the transcription buffer), except with 250 μM added phosphorothioate nucleotide and no inhibitor oligo, then quenched with 50 mM EDTA, centrifuged twice through 10× the reaction volume of Sephadex G25 resin preincubated in 10 mM Tris-HCl buffer, and subjected to [^{32}P] pCp 3′ end-labeling.

End-labeling reaction consisted of equal parts 10X T4 Ligase RXN Buffer (Invitrogen) buffer supplemented with ATP, DMSO (Sigma), 100 mM DTT, and 100 μM inhibitor oligonucleotide, along with 10 μCi of [^{32}P] pCp (Perkin-Elmer), 10 units of T4 RNA ligase (Invitrogen), and the G25 purified RNA. Reaction was incubated at 37 °C for approximately one hour, then subjected to denaturing PAGE purification. Bands corresponding to both full-length and self-cleaved versions of the ribozyme in each phosphorothioate-substituted nucleotide were excised, eluted in water, and G25 purified again. The purified RNA was then mixed with kinetic reaction buffer and a small amount of iodoethanol to induce cleavage of the phosphorothioate-substituted RNA backbone. RNA was incubated at ambient temperature for approximately five minutes, mixed with equal volumes of gel loading buffer, and separated by 15% denaturing PAGE purification prior to analysis of resulting radiographic cleavage pattern.

7. In-Line Probing. RNA was transcribed as described above for three hours at 37 °C, then isolated using 7.5% denaturing PAGE. Excised bands were eluted for up to two hours in 0.3 M KCl, and EtOH precipitated overnight.

The resulting RNA pellet was resuspended in 20 μL water, and mixed with 10× T4 RNA ligase buffer, DMSO, 100 μM inhibitor oligo, 10 μCi of [^{32}P] pCp, and 10 units of T4 RNA ligase. This reaction was incubated for one hour at 37 °C and purified on 7.5% denaturing PAGE, eluted in water for one hour, and subjected to G25 resin. RNA was then mixed with appropriate concentrations of Mg^{2+} or Ca^{2+} in kinetics reaction buffer, and allowed to incubate at 37 °C for approximately 48 h.

Following incubation, RNA was fractionated on a 15% denaturing PAGE apparatus prior to radiographic analysis. The RNA sequence was determined by identifying the strong

dx.doi.org/10.1021/bi401717w | Biochemistry 2014, 53, 1616−1626

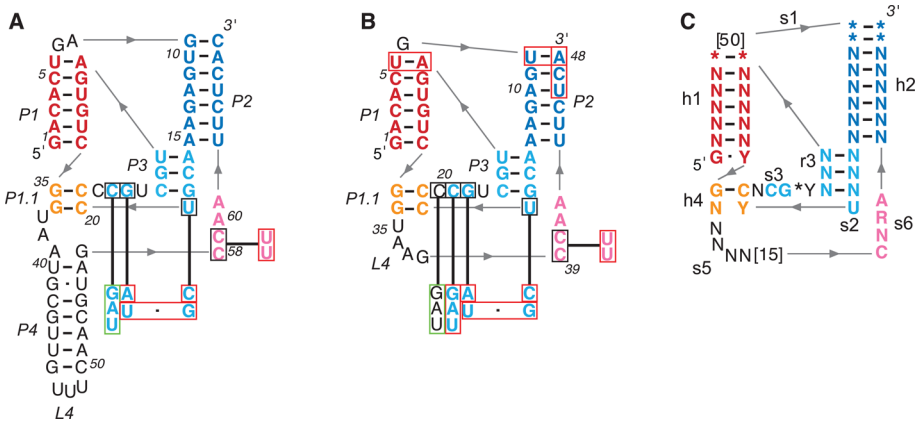

Figure 1. Minimization of HDV-like ribozymes. (A) drz-Spur-3 ribozyme. Black boxes indicate sites of mutagenesis, with connected boxes indicating variants. Green and red boxes indicate permissive and inhibitory substitutions, respectively. (B) Minimized drz-Spur-3 ribozyme (drz-Spur-3-min). Color scheme for substitutions is the same as in (A). Nucleotides in red boxes indicate deletions that abolished self-scission. (C) Structure-based descriptor used in genomic searches for minimal HDV-like ribozymes. Asterisks indicate nonessential insertions. Bracketed numbers correspond to variable-length regions with maximum lengths indicated in the brackets.

cleavage bands seen in the displayed in-line reaction in the L4 loop region as the same bands that appeared when the samples were run next to phosphorothioate sequencing ladders.

RESULTS

Minimization of drz-Spur-3 and Structure-Based Searches. In order to determine the minimal sequence required for an HDV-like ribozyme activity, a series of deletions were designed based on the drz-Spur-3 ribozyme. This ribozyme was chosen because it exhibited robust cleavage activity even thought it contained a shortened six base-pair P1 helix (Figure 1A).[16] Furthermore, the drz-Spur-3 ribozyme maintains the sequence requirements important for self-scission in the HDV-like fold: mutations of the active site cytosine (C58) abolish activity and self-scission is abrogated when the U19•G24 reverse wobble pair at the base of the P3 helix is either swapped or individually mutated to form traditional Watson−Crick base-pairs (U19C or G24A).[2,4,5,23,24] When we mutated the G-U pair in drz-Spur-3, self-scission was abolished, supporting an interaction similar to the genomic HDV ribozyme.[5] Interestingly, mutations to the C23 residue in drz-Spur-3 showed minimal effect on self-scission. This nucleotide is highly conserved in the HDV ribozyme, and it extends the P3 helix by stacking on the reverse G•U wobble in HDV ribozyme crystal structures.[2,5,21,23] Overall, these data support a model of the drz-Spur-3 ribozyme core highly similar to the HDV ribozyme, while the reduced P1 helix made it an ideal candidate for minimization studies.

We started minimization of the drz-Spur-3 ribozyme by investigating the P4 helix. Previous reports indicated that this helix is not essential, and can be replaced with an eight-nucleotide loop without abolishing catalysis.[21] To test whether this reduction has the same effect on the drz-Spur-3 sequence, we sequentially deleted nucleotides in this region until only four nucleotides joined the P1.1 helix to the active site cytosine. The composition of these nucleotides appears unimportant, as both the wild-type UAAG sequence as well as a GAAA mutant supported self-scission. Shortening this strand further to a three-nucleotide joining region abolished self-cleavage.

We next sought to examine the nucleotide requirements in the P1, J1/2, and P2 regions of the ribozyme. Several HDV-like ribozymes contain only a single nucleotide in the J1/2 region, and indeed this length was tolerated in the drz-Spur-3 sequence with no compositional preference, despite the presence of the shorter P1 helix.[18] The P2 helix was less susceptible to deletions, as removal of more than a single base-pair abolished activity. Deletions to the 3′ side of this helix also proved deleterious to self-scission. Finally, further shortening of the P1 helix failed to yield active constructs, even in conjunction with additional reductions to the P2 helix on the expectation that similar helical length for the P1 and P2 regions would maintain the same register along the two helical stacks. Combined, these deletions yielded a 48-nt minimal motif, drz-Spur-3-min, which possessed residual cleavage activity ($3 \times 10^{-3} \pm 1 \times 10^{-3}$ min^{-1}, 37 °C and 10 mM Mg^{2+}) (Figure 1B).

To verify that the minimized ribozyme, drz-Spur-3-min, was undergoing HDV-like self-scission, we again mutated residues predicted to be essential to catalysis. A C39U/C40U double mutation abolished self-scission, as did reversal of the predicted G•U wobble pair at the base of the P3 helix. Unlike the drz-Spur-3 parent sequence, mutation of the C21 residue that stacks on the G•U wobble was detrimental to self-scission. However, mutations to C20, which is predicted to act only as a spacer nucleotide, did not affect catalysis. These results indicate that the drz-Spur-3-min ribozyme, despite being only 48 nucleotides long, maintains the HDV-like ribozyme core.

Using the drz-Spur-3-min sequence as the template, we designed secondary-structure descriptors to use in searches for minimal genomic HDV-like ribozymes (Figure 1C).[25] Because the minimal HDV-like motif, as defined by drz-Spur-3-min, contained several features that were excluded when HDV-like ribozymes were first identified through structure-based searches, we allowed the P1 helix to be six or seven base pairs long, and the J1/2 and P4/L4 regions to be up to 50 and 19 nucleotides in length, respectively. We searched through the available genomic sequences of viruses, bacteria, and eukaryotes, as well as a several microbial metagenomic data sets for sequences capable of forming the minimal HDV-like secondary structure. The result was a relatively permissive structure-descriptor that uncovered numerous putative HDV-like ribozymes that possessed some or all of the newly defined minimal features. Of particular interest were a family of sequences found in the lancelet *Branchiostoma floridae*, where canonical HDV-like ribozymes were previously found, a

dx.doi.org/10.1021/bi401717w | *Biochemistry* 2014, 53, 1616−1626

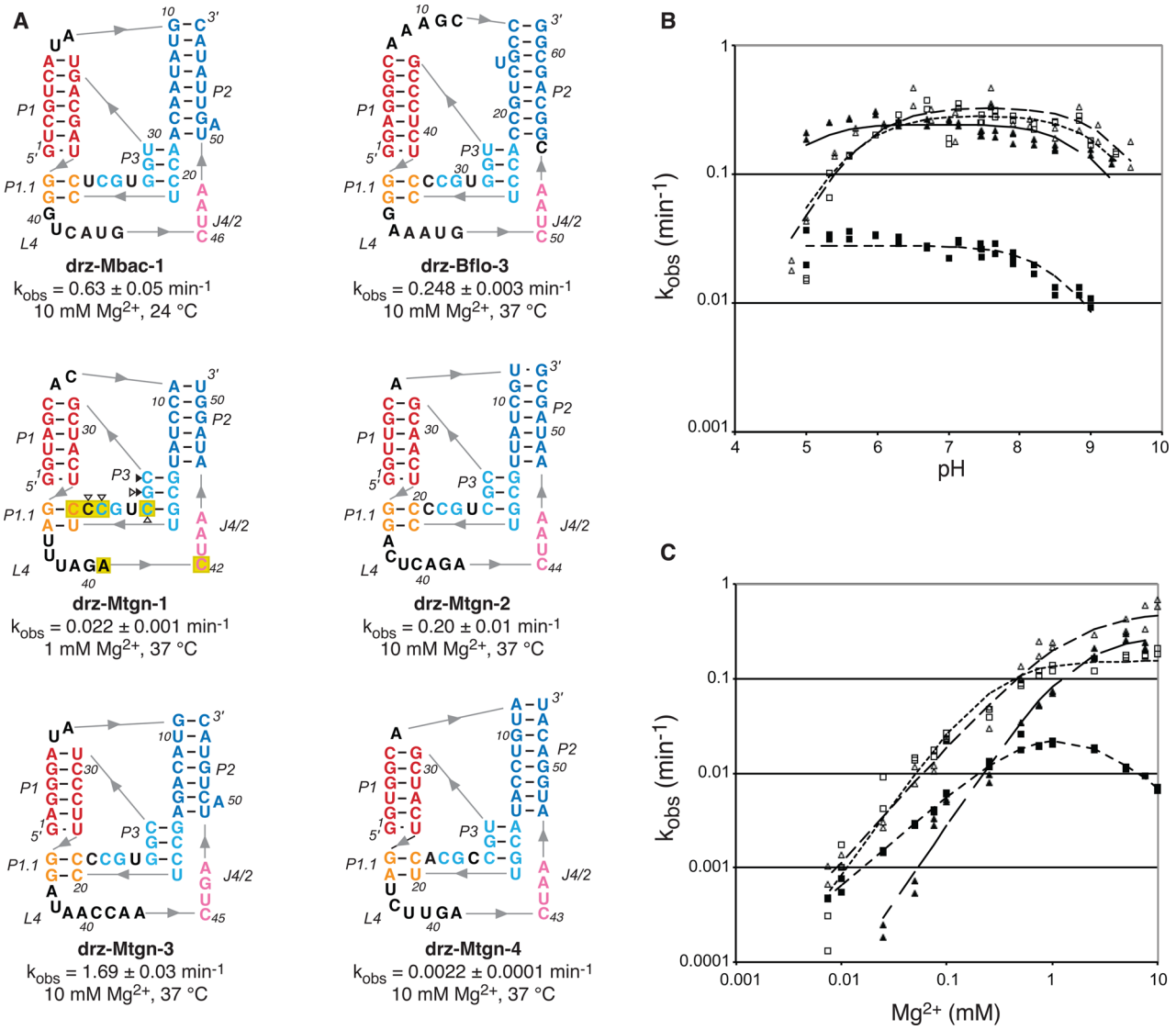

Figure 2. Minimal HDV-like ribozymes. (A) Secondary structures and activity of the genomic minimal HDV-like ribozymes, drz-Mbac-1, drz-Bflo-3, drz-Mtgn-1, 2, 3, and 4, respectively. Nucleotides boxed in yellow in the drz-Mtgn-1 ribozyme correspond to positions subject to phosphorothioate interference shown in Figure 4, closed arrows correspond to positions subject to in-line degradation at low Mg^{2+}, and open arrows correspond to positions showing in-line degradation at high Mg^{2+} concentrations. (B) pH profiles of the drz-Mbac-1 (open triangles), drz-Bflo-3 (filled triangles), drz-Mtgn-1 (filled squares), and drz-Mtgn-2 (open squares) ribozymes. The estimated pK_as for each ribozyme are 5.7 and 9.4, 4.7 and 9.0, undefined and 8.6, and 5.6 and 9.2, respectively. (C) Mg^{2+}-dependence of the ribozymes. Symbols are the same as in (B). The calculated Mg^{2+} $K_{1/2}$s are 1.5 mM, 1.7 mM, 1.0 mM, and 0.28 mM, respectively.

ribozyme from *Mollicutes* bacterium D7 (also known as *Coprobacillus* sp. D7), and a number of sequences identified in a metagenomic data set derived from the human microbiome (Figure 2).[16,22] The metagenomic ribozymes represent the smallest naturally occurring HDV-like ribozymes.

Characterization of Minimal HDV-Like Ribozymes. In the lancelet *B. floridae*, three minimal HDV-like ribozymes were found in close proximity to each other. This organism was previously shown to harbor two families of canonical HDV-like ribozymes (drz-Bflo-1 and -2).[16] The new drz-Bflo-3 family is characterized by a seven base-pair P1 helix and a five nucleotide J1/2 region. Unlike the extended J1/2 domains found in the drz-Agam-2 ribozymes and related retrotransposon-associated HDV-like ribozymes, no secondary structure is predicted for the J1/2 region of the drz-Bflo-3 sequences.[16,26−28] The drz-Bflo-3 family also lacks the entire P4 helix, instead employing just six nucleotides to join the P1.1 helix to the active-site cytosine. Mutation of the active site cytosine to a uridine abrogated self-scission, confirming an HDV-like catalytic core.

The three drz-Bflo-3 ribozymes identified through structure-based searches reside on the same strand within a 4000-nucleotide region of a single genomic scaffold. No annotated transcripts are present in this locus, although several ESTs are found within 20 kb of the ribozymes. Sequence-based searches of the *B. floridae* genome revealed three additional drz-Bflo-3-like ribozymes. Two of these sequences contain four point mutations, none of which are predicted to lower the ribozyme activity; however, the third instance lacks a fully base-paired P2 helix. Notably, the drz-Bflo-3−5 sequence resides within a large intronic region of EST 869853, which is predicted to code for the catalytic core domain of a cysteinyl tRNA synthetase, but the ribozyme's function within this intron is unknown.

Microbial Ribozymes. Two strains of the *M. bacterium* were found to harbor a single copy of a small HDV-like

dx.doi.org/10.1021/bi401717w | *Biochemistry* 2014, 53, 1616−1626

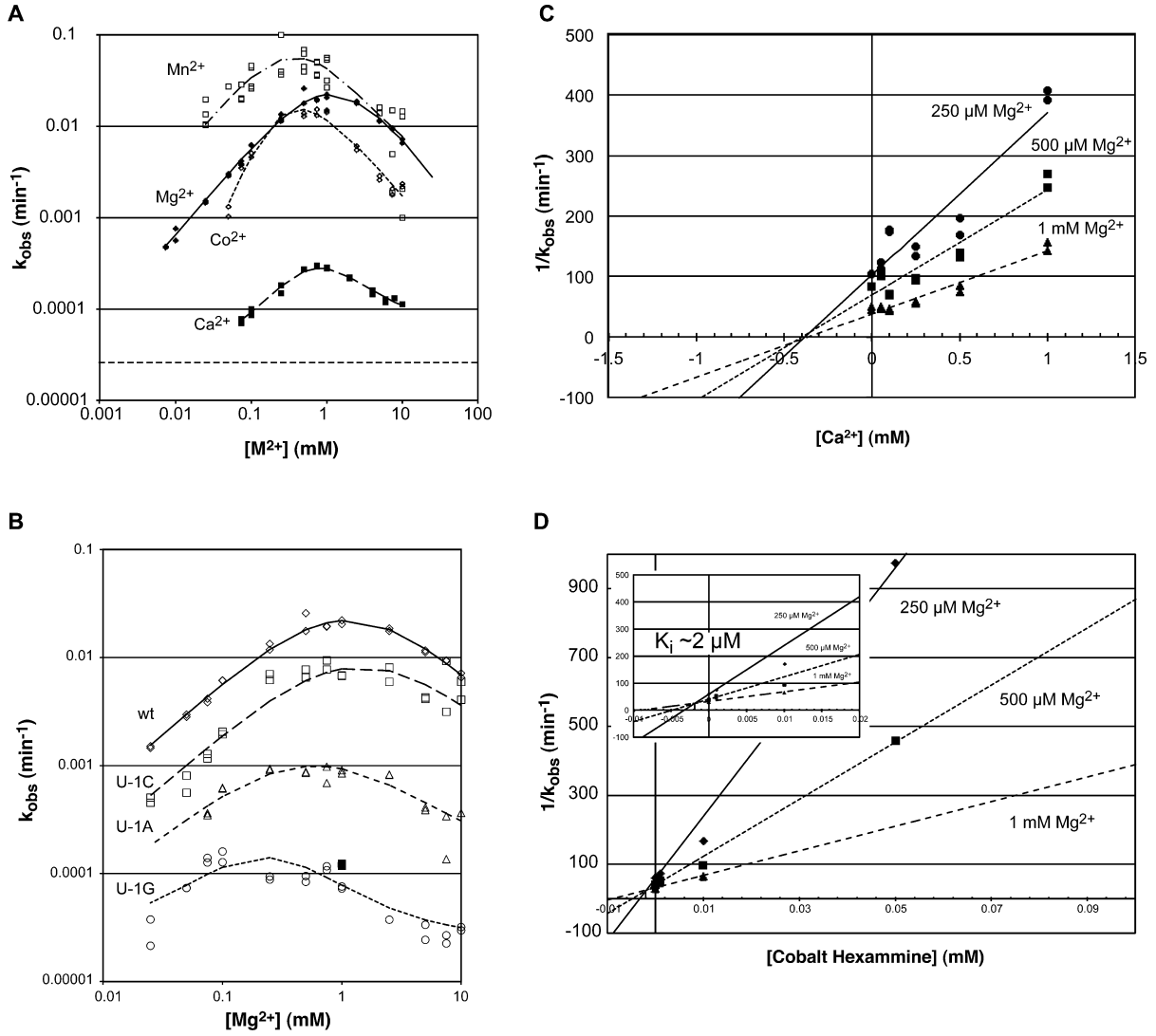

Figure 3. *In vitro* activity of the drz-Mtgn-1 ribozyme. (A) Divalent metal ion profile of the drz-Mtgn-1 ribozyme. The calculated $K_{1/2}$s for Mg^{2+} (filled diamonds), Mn^{2+} (open squares), Co^{2+} (open diamonds), and Ca^{2+} (filled squares) are 0.96 and 1.3, 0.23 and 0.51, 0.26 (Hill coefficient ~1.9) and 0.53, and 0.58 and 2.0, respectively, at 37 °C, in 140 mM KCl and 10 mM NaCl. The dashed line corresponds to the observed rate of cleavage in the absence of divalent metal ions. (B) Mg^{2+} response of the WT (diamonds) and U-1 variant ribozymes with U-1A (triangles), U-1C (squares), and U-1G (circles) substitutions. The bell-shaped response suggests that the -1 nucleotide does not affect binding of additional, rate-reducing metals (see Discussion). The activity for the U-1G mutant in calcium (filled squares) suggests that the low activity for the WT sequence in Ca^{2+} is due to unfavorable interactions Ca^{2+} forms with the upstream nucleobase. (C) Ca^{2+} inhibition of the Mg^{2+}-dependent activity. The intersection point for linear models for $1/k_{obs}$ at 250 μM (circles), 500 μM (squares), and 1 mM (triangles) Mg^{2+} over a range of Ca^{2+} concentrations indicate noncompetitive (allosteric) inhibition with a Ca^{2+} K_i of ~400 μM. (D) Cobalt hexammine inhibition of the Mg^{2}-dependent activity. The intersection point for linear models for $1/k_{obs}$ at 250 μM (circles), 500 μM (squares), and 1 mM (triangles) Mg^{2+} over a range of cobalt hexammine concentrations indicates competitive inhibition with a K_i of ~2 μM. Displayed values are the average of two independent trials.

ribozyme that contains a two-nucleotide J1/2 region, a seven base-pair P1 helix, and a six-nucleotide L4 loop. The ribozyme self-cleaved efficiently at ambient temperature in physiological-like metal ion concentrations (0.23 ± 0.01 min^{-1}; 24 °C and 1 mM Mg^{2+}). Drz-Mbac-1 resides ~700 nts downstream of a predicted PolY gene (EHM88375) and ~300 nt upstream of several other predicted genes of unknown function (EHM88373 and EHM88374) as well as $tRNA^{Met}$. This sequence represents the second confirmed bacterial HDV-like ribozyme, suggesting that HDV-like ribozymes may be more common in bacteria than originally found.[16]

Several small HDV-like ribozymes were identified in metagenomic data sets, which were derived from deep sequencing of human sewage and previously yielded 14 new hammerhead ribozymes.[22,29−31] Four of these (drz-Mtgn-1 to 4) were active *in vitro*, showed no self-scission when the active site cytosine is mutated to a uridine, and exhibited remarkably small HDV-like structures. In particular, drz-Mtgn-1 consists of the minimal P1 and P2 helices of six base-pairs seen in the engineered minimal ribozymes, along with only two nucleotides in the J1/2 region and six nucleotides joining the P1.1 to the active site cytosine, and self-cleaves with a rate constant of (0.021 ± 1) × 10^{-3} min^{-1} in 1 mM Mg^{2+} at 37 °C.

The sequencing tracks containing drz-Mtgn-1 and -4 were obtained from a human diarrheal sample and exhibited partial overlap, indicating that these ribozymes occur in a single organism. Drz-Mtgn-4 also lacks a P4 helix, but has a predicted 8-bp P2 helix, self-cleaves with a rate constant of (2.0 × 10^{-3})

dx.doi.org/10.1021/bi401717w | *Biochemistry* 2014, 53, 1616−1626

± (1×10^{-4}) min^{-1} in 10 mM Mg^{2+} at 37 °C, and appears in the metagenomic contig In-A_000423 (GenBank BABB01000423.1). The sequencing track from which drz-Mtgn-1 was isolated shows similarity to a locus of the *Bacteroides cellulosilyticus* gene coding for a 3-deoxy-7-phosphoheptulonate synthase, with the ribozyme located approximately 400 nts upstream of the protein-coding domain.[32] This mapping suggests that the drz-Mtgn-1 and -4 ribozymes originated from a bacterial genome.

The drz-Mtgn-2 and -3 ribozymes shared similar structural features with drz-Mtgn-1 and -4; however, they possess 7-bp P2 helices and slightly longer joining strands between the P1.1 helix and the active-site cytosine. These sequences self-cleave faster than the drz-Mtgn-1 and 4 ribozymes (k_{obs} = 0.20 ± 0.01 min^{-1} for drz-Mtgn-2; 1.69 ± 0.03 min^{-1} for drz-Mtgn-3 in 10 mM Mg^{2+} at 37 °C), on par with many larger HDV-like ribozymes.[16] The drz-Mtgn-2 ribozyme, like the drz-Mtgn-1 and -4 sequences, was identified in a human diarrheal sample, whereas drz-Mtgn-3 was obtained from deep sequencing of human sewage.

Kinetic pH Profiles. To probe the effects of the minimal HDV-like structures on the catalytic mechanism, we examined pH profiles for the most active constructs (Figure 2B). This analysis was conducted in physiological monovalent ion concentrations (140 mM KCl, 10 mM NaCl), which was previously shown to reduce the apparent pK_a of the catalytic cytosine in the HDV ribozymes.[33] All of the tested small HDV-like ribozymes, along with the full-length drz-Spur-3 sequence, exhibited flat pH profiles between pH 6 and pH 8, consistent with a mechanism in which two titratable groups affect the rate-limiting step of the reaction. However, neither the drz-Bflo-3 family nor the drz-Mtgn-1 ribozyme showed a decline in activity at lower pH, suggesting a pK_a for the active-site cytosine comparable to the unperturbed value of ∼4.2, and likely resulting from the presence of 150 mM monovalent salts.[34]

In addition to the activity−pH relationship, we examined the divalent metal ion dependence of the minimal ribozymes, along with the drz-Spur-3 sequence (Figure 2C). The drz-Spur-3, drz-Bflo-3, drz-Mbac-1, and drz-Mtgn-2 ribozymes all showed a strong metal dependence up to 10 mM Mg^{2+}. The Hill coefficients for these sequences varied between 1 and 1.6, indicating some binding cooperativity, as was previously suggested for the HDV and *CPEB3* ribozymes.[17,33] Again, the moderately high physiological-like levels of monovalent ions included in the buffer solution likely partially stabilized the active structure, perhaps resulting in slightly lower Hill coefficient than would be observed in a monovalent ion-free solution. In all cases the self-scission followed a monoexponential decay. Biexponential behavior, typical of larger HDV-like ribozymes and indicative of misfolded ribozyme subpopulations, was not observed for any of the constructs.

Metal Dependence and Role of the Upstream Nucleobase on drz-Mtgn-1 Scission. Surprisingly, the drz-Mtgn-1 ribozyme did not show an increase in its catalytic rate constant at higher Mg^{2+} concentrations. This ribozyme exhibited a positive activity−metal correlation up to ∼1 mM Mg^{2+}, but at higher concentrations, cleavage rate constants decreased, resulting in bell-shaped activity−metal curves. A parsimonious explanation for this pattern is a model with two metal-binding modes, one of which promotes fast catalysis and a second that either inhibits catalysis or causes it to proceed at a much slower rate. A similar model was previously used to explain hammerhead ribozyme cleavage in the presence of lanthanides, and a related metal ion response has been observed for both genomic and anti-genomic HDV ribozymes with distinct combination of metal ions and the nucleotide identity at the -1 position, though not with Mg^{2+} as the catalytic metal.[9,15,35]

To further study the bell-shaped metal dependence of the drz-Mtgn-1 ribozyme, its self-cleavage activity was analyzed with a panel of divalent metal ions. The activity of the drz-Mtgn-1 ribozyme in the tested metal ions was variable, but did not follow any physiochemical trends, such as pK_a or the ionic radius. Unlike HDV ribozymes, drz-Mtgn-1 exhibited bell-shaped activity−metal curves for all divalent ions tested, suggesting that the second metal-binding mode for this ribozyme is inherent to the fold and not a product of a particular metal's unique interaction with the ribozyme's structure (Figure 3A). These results agree with a two-channel model for self-cleavage, wherein at low divalent metal concentrations only the catalytic metal-binding site is occupied and self-scission proceeds efficiently, but as the concentration of divalent ions increases, the metal ion binds an additional site that promotes a suboptimal conformation, causing the observed cleavage rate to decrease.[8,15] We also observed that the self-scission in Ca^{2+} proceeded approximately 100-times slower than in other divalent metals. Such a pronounced preference against a particular divalent metal has not been seen in other HDV-like ribozymes, including the full-length drz-Spur-3 sequence. Calcium dependence retained a bell-shaped metal-response curve, indicating that it could bind in both rate-activating and rate-reducing modes; however, the absence of efficient catalysis suggests that Ca^{2+} interacts with the ribozyme in a profoundly different manner than the other tested divalent metals.

We next sought to examine the Ca^{2+} dependence further by constructing variants with U-1A/C/G mutations, because in HDV ribozymes the identity of the nucleotide immediately upstream of the cleavage site was previously shown to influence the metal ion dependence and results in a bell-shaped k_{obs} plot.[15] These constructs exhibited highly variable kinetics in Mg^{2+}, with the U-1C construct cleaving at approximately the same rate as the wild-type sequence, and the U-1A and U-1G mutants cleaving ∼100-times more slowly (Figure 3B). These data agree with previous analysis of the -1 position's effect on self-scission in HDV ribozymes.[12,14] However, all drz-Mtgn-1 U-1 constructs continued to exhibit a bell-shaped metal dependence in Mg^{2+}, although for the U-1G construct, it was less pronounced. The slow self-scission of the U-1G mutant, coupled with the low metal response, correlates with previous models of the genomic HDV ribozyme active site, where the larger guanosine base is unable to assume the proposed U-turn kink that leads to efficient metal binding and is necessary for fast self-scission.[12,13] As the U-1A construct also self-cleaved slowly, it is likely that a purine base at this site in general impairs metal binding, leading to slow catalysis. Because substitutions at the -1 nucleotide did not alter the overall shape of the activity−metal curves, the proposed second metal-binding mode appears independent of the upstream nucleotide; instead, this secondary binding mode seems to influence the core of the ribozyme.

The rate of self-scission for the U-1G construct was similar to the rate of self-cleavage of drz-Mtgn-1 in the presence of Ca^{2+}, suggesting that relatively slow cleavage in the presence of Ca^{2+} could be due to the metal's interaction with the -1 nucleotide. To test this model, we measured the self-cleavage for the U-1G

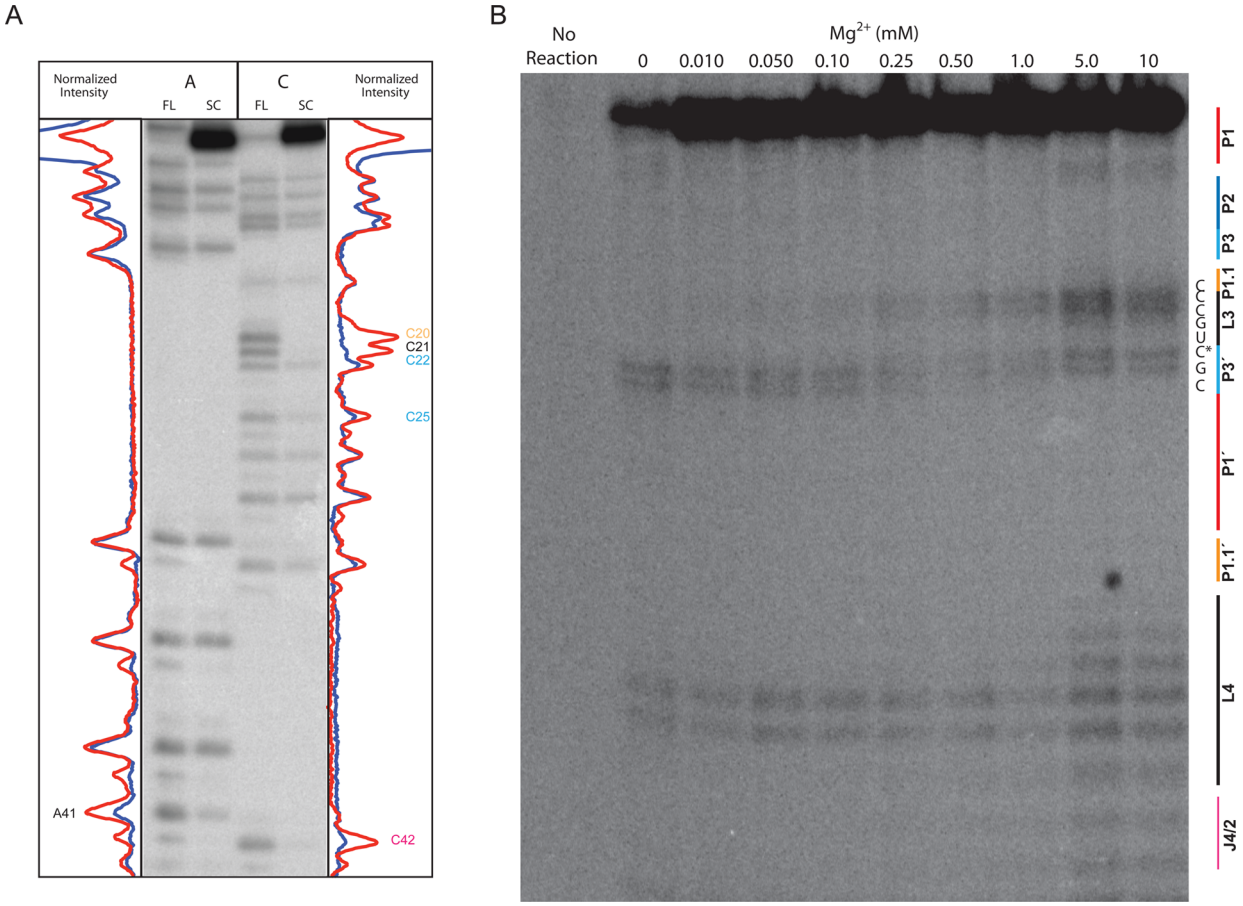

Figure 4. Structural analysis of drz-Mtgn-1. (A) Phosphorothioate interference mapping of A and C positions in the drz-Mtgn-1 ribozyme under cotranscriptional conditions. FL corresponds to full-length ribozyme and SC indicates the self-cleaved fraction. The normalized intensity for the A and C nucleotides are displayed to the left and right, respectively, with the red traces corresponding to the FL lanes, and the blue traces corresponding to the SC lanes. Positions demonstrating enrichment in the FL fraction are indicated and colored as in Figure 2. (B) In-line probing of the drz-Mtgn-1 sequence under increasing magnesium concentrations. No reaction corresponds to drz-Mtgn-1 RNA that was not subjected to in-line degradation and contains a full length, precursor form of the ribozyme (not shown). The various domains comprising the ribozyme's structure are indicated and colored as in Figure 2. The asterisk indicates the position where the degradation pattern shifts by a single nucleotide between low and high Mg^{2+} regimes. The sequence for the displayed PAGE is correlated with the appearance of the strong cleavage points in the L4 region in independent sequencing experiments (see Figure S1).

mutant in the presence of Ca^{2+} and compared it to the rate obtained for this construct in the presence of Mg^{2+} (Figure 3B). Unlike in the wild-type drz-Mtgn-1 ribozyme, where cleavage occurs roughly 100-times slower when calcium is present instead of magnesium, there is almost no difference in scission between these two metals in the U-1G construct. If the slow self-scission for the wild type ribozyme in calcium was due to the metal's interaction with a region other than the nucleotide upstream of the cleavage site, the U-1G mutant would be expected to also cleave more slowly in calcium. That is, the effect of the metal ion and U-1 mutation on the cleavage rate would be additive. Because the U-1G ribozyme rate constants in Mg^{2+} and Ca^{2+} are almost identical, the slow self-scission of the wild type ribozyme in Ca^{2+} is likely due to formation of a nonproductive conformation around the -1 nucleotide when calcium is the only divalent metal present.

Ca^{2+} Inhibition of drz-Mtgn-1 Activity. Because drz-Mtgn-1 cleaved slowly in Ca^{2+}, we sought to test whether Ca^{2+} affects the self-cleavage reaction in the presence of Mg^{2+}. We measured the ribozyme scission at various concentrations of Ca^{2+} and Mg^{2+}, and the inverses of the observed rates were plotted against the concentration of Ca^{2+}, yielding the Dixon plot for inhibition analysis. A fundamental assumption of the Dixon analysis is that the rate of catalysis increases as the nontitrated reactant is increased. This method of inhibition analysis was only valid for Mg^{2+} concentrations below 1 mM, because above 1 mM Mg^{2+}, additional magnesium reduced the observed rate (Figure 3A). At low Mg^{2+} concentrations, cleavage is reduced in the presence of Ca^{2+} and the inhibition appears to be noncompetitive with a K_i of approximately 400 μM, whereby the Ca^{2+} ion binds at a site other than the active site and prevents fast catalysis (Figure 3C). Whether this effect is a result of calcium's presumed interaction with the nucleotide upstream of the cleavage site, or calcium interfering with other, noncatalytic magnesium binding sites, cannot be distinguished. In a control experiment, a titration of cobalt hexammine, an exchange-inert isostere of hydrated Mg^{2+}, produced a Dixon plot suggesting competitive inhibition over the same concentrations of Mg^{2+}, as has previously been reported for the HDV ribozyme (Figure 3D).[36] This result indicates that, at low concentrations, Mg^{2+} forms the same interactions within the active site of drz-Mtgn-1 as in the HDV ribozymes.

The Dixon analysis cannot be used over Mg^{2+} concentrations that yield decreasing cleavage rates in the absence of calcium;

dx.doi.org/10.1021/bi401717w | *Biochemistry* 2014, 53, 1616−1626

however, information regarding metal binding can still be inferred. When Ca^{2+} is present at concentrations greater than 1 mM in reactions over this range of Mg^{2+} concentrations, rate constants are found to increase with additional Mg^{2+}, contrary to what occurs in the absence of Ca^{2+}. Below this calcium threshold, rate constants again decrease with rise of Mg^{2+} concentration. The calcium concentration at which this inversion occurs can be observed on a Dixon plot at the intersection point of the linear fits for calcium inhibition in higher Mg^{2+} regimes. In 1, 5, and 10 mM Mg^{2+}, linear fits cross at ~300 μM, which agrees well with the estimated K_i from rate-enhancing Mg^{2+} regimes. This result suggests that the primary cause of reduced catalysis at elevated Ca^{2+} and Mg^{2+} concentrations is likely due to a large population of the ribozyme forming an inactive fold (e.g., a misfolded U-turn) that is rescued when increasing amounts of Mg^{2+} displace calcium binding. At the lower Ca^{2+} concentrations, the inactive population arising from Ca^{2+} interactions is smaller, and the primary factor contributing to reduced catalysis is auto-inhibition due to increasing Mg^{2+} levels occupying a second binding site, leading to inefficient catalysis. In combination, the calcium inhibition patterns in various magnesium regimes support a model in which calcium promotes formation of a nonproductive fold near the scissile phosphate, precluding efficient Mg^{2+}-catalyzed scission, and both metals retain dual binding modes that result in autoinhibition at elevated metal ion concentrations.

Structural Mapping of drz-Mtgn-1. In order to further define the bell-shaped metal profiles of drz-Mtg-1, we sought to probe its metal-binding sites. To begin, we performed phosphorothioate interference mapping, in which the pro-R_p oxygen was substituted with a sulfur to define regions of the backbone where oxygen atoms are required for catalysis, either by binding a metal or by forming interactions with other regions of the ribozyme to help stabilize the active conformation.[37] Phosphorothioate substitution revealed several positions in the phosphate backbone essential for catalysis during cotranscriptional self-cleavage in the presence of Mg^{2+} (Figure 4A). Bands corresponding to thiophosphate-substituted nucleotides around the active site, as well as cytosines in the P1.1 and L3 core, were enriched in the inactive species of ribozyme (see Figure 2A for mapping of the interference sites onto the secondary structure). These regions correspond to known sites of Mg^{2+} binding in the HDV ribozymes and overlap with sites of phosphorothioate interference in the genomic HDV and human *CPEB3* ribozymes, suggesting that drz-Mtgn-1 ribozyme forms the conserved HDV ribozyme active site, despite the reduction in secondary structural elements.[5,17,38] While this interference pattern supports a model wherein a single or multiple Mg^{2+} ions are forming contacts to the backbone around the active site prior to efficient catalysis, it failed to differentiate between the conformational changes that lead to subtle rate differences in active species under changing metal concentrations.

Ribozyme activity depends on the ability of the sequence to assume the catalytically competent conformation. Such folds are highly structured, and consequently, the phosphate backbone exhibits defined susceptibility to in-line degradation.[39,40] The varied activity under changing Mg^{2+} concentrations seen for the drz-Mtgn-1 sequence indicates that the ribozyme is capable of forming multiple folding states. These states likely correspond to different backbone segments forming stable structures, and thus, analysis of the backbone for its propensity to in-line attack under changing metal levels reveals sites of metal-dependent reorganization of local structure.

When the drz-Mtgn-1 ribozyme was incubated at various concentrations of Mg^{2+}, several regions exhibited changing degradation patterns (Figure 4B). At low magnesium levels, backbone scission is observed in the 3′ side of the P3 helix as well as the L4 loop region. With increasing Mg^{2+} concentration yielding the fastest self-cleavage rates, the bands corresponding to the loosely structured L4 loop remained susceptible to in-line attack; however, the bands corresponding to the P3 domain diminished, indicating the formation of a stable helix. When Mg^{2+} was present at levels where autoinhibition was observed, extensive degradation is seen throughout the J4/2 and L4 regions. Significantly, a single-nucleotide shift occurs in the 5′ direction from the degradation pattern observed for the P3 helix at low Mg^{2+} concentrations, corresponding to a stabilized cytosine at the top of the helix and a labile cytosine at the base of P3 adjacent to L3 (Figures 2A, 4B, and S1). Furthermore, new bands mapping to the two cytosines in the L3 domain appear at high Mg^{2+}. Combined, these changes in cleavage patterns correlate well with the observed kinetic data: breakdown in P3 motif decreases from low Mg^{2+} levels to the concentrations yielding the fastest self-scission, corresponding to the formation of a stable helix, whereas above these Mg^{2+} levels, degradation products appear in the L3 and P3 domains indicating a rearrangement of the catalytic core at higher metal concentrations.

■ DISCUSSION

We have defined the minimal sequence needed for self-scission by an HDV-like motif to be just 48 nucleotides, and used this minimal motif to identify small HDV-like self-cleaving sequences throughout genomic space. The structure descriptors allowed for several variants of the minimal motif, uncovering numerous putative ribozymes. These included a sequence family in *B. floridae*, an organism that appears to be rich in HDV-like self-cleaving sequences, and several examples of microbial origin.

The drz-Bflo-3 family represents the third structurally unique HDV-like family of ribozymes found in the lancelet genome. This family differs significantly from the drz-Bflo-1 and 2 sequences in that they contain an extended J1/2 domain and no P4 region. The close proximity of the three drz-Bflo-3 ribozymes raises questions regarding their biological function, which is presently unknown. A similar arrangement of HDV-like ribozymes was found in the *S. purpuratus* drz-Spur-1 family;[16] however, in this organism the ribozymes are found within a single intron or UTR, whereas we found no annotated genes near the drz-Bflo-3 family. Given that the drz-Bflo-3 family of ribozymes is found to be highly conserved throughout the *B. floridae* genome, as well as the broad distribution of the drz-Bflo-1 and 2 families within *B. floridae* genome, it is likely that this organism harbors repeat elements that employ the ribozymes in a manner analogous to that seen in many other ribozyme-terminated retrotransposons.[26−28]

The majority of the minimal HDV-like ribozymes were discovered in microbial genomes, contrasting with previous studies which identified larger HDV-like ribozymes primarily in multicellular eukaryotes, with single examples identified in an insect virus, a human gut bacterium, and a marine unicellular diplonemid.[16−18] Whereas many eukaryotic ribozymes are associated with retrotransposons,[26−28] the microbial examples do not appear to have a uniform biological function informed

by their genomic loci. Further analysis of the effect that these elements have on the expression of surrounding genes will likely reveal the biological roles of these ubiquitous catalytic RNAs.

The HDV-like ribozymes found in human metagenomic samples are the smallest confirmed HDV-like self-cleaving sequences. Although sequence homology is only confirmed for the contig on which the drz-Mtgn-1 motif is found, it is likely that all of these ribozymes are of viral or bacterial origin. The ribozymes, along with the drz-Mbac-1 sequence, expand the number of microbial HDV-like ribozymes and indicate that this class of RNAs is widespread in bacteria, and suggest that the fold may be ancient in origin.

Metagenomic data sets have proven highly valuable in identifying self-cleaving ribozymes. Previously, a number of examples of hammerhead ribozymes were obtained from analysis metagenomic sequence tracks,[31] and now several HDV-like ribozymes have been found in similar metagenomic samples. This finding indicates that the usefulness of these types of sequence repositories extends beyond the mapping of viral and bacterial populations, as they provide highly diverse data sets rife with functional RNAs.

The metagenomic ribozymes exhibited an array of cleavage rate constants, despite very similar sequence composition. As a whole, the rates of self-scission for these metagenomic ribozymes suggest that the optimal orientation for linking of a 6-bp P1 domain to the P2 helix in the context of the HDV-like fold occurs when the P2 helix is 7 bp long and the J1/2 strand consists of two nucleotides. Such an arrangement is observed in the drz-Spur-3 sequence, and the fast-acting drz-Mtgn-3 ribozyme described here.

Among the minimal ribozymes analyzed in this study, the drz-Mtgn-1 proved to be most unusual. The presence of two distinct titration points in the metal-activity relationship and the marked preference against Ca^{2+} as the catalytic metal was not expected for an HDV-like self-cleaving sequence, because these ribozymes typically show robust activity in any divalent metal.[41] In-line probing showed that the smallest HDV-like self-cleaving sequence can sample several conformational states that are biased by the divalent metal ion concentrations and are absent in larger examples of the class. The mapping experiment suggested that these conformational states arise from direct perturbations to the ribozyme core, particularly around the P3 and L3 domains.

The drz-Mtgn-1 ribozyme also exhibits Ca^{2+} modulation of the Mg^{2+}-dependent self-scission reaction, resulting in a unique metal-activity profile for the combination of these two ions. The rate modulation caused by Ca^{2+} correlates well with the observed K_ds for each metal individually, as the inhibitory effect is greatest when the Mg^{2+} concentration is below its predicted K_d for the active site and the Ca^{2+} concentration is in the millimolar range. The noncompetitive nature of inhibition indicates that calcium does not interfere with magnesium binding in the catalytic pocket; instead, Ca^{2+} appears to bind another location, likely in the leader sequence just upstream of the cleavage site, in a manner that that prevents efficient self-scission.

The biological roles of HDV-like ribozymes have not been characterized outside of retrotransposons and the hepatitis delta virus, but the unique metal-ion dependence of the drz-Mtgn-1 ribozyme may allow for modulation of its activity by calcium. Calcium levels are tightly regulated in cells and can increase dramatically during signaling events.[42] Elevated calcium levels inhibit self-scission of the drz-Mtgn-1 ribozyme, potentially affecting downstream events coupled to the ribozyme activity and linking calcium signaling with ribozyme activity.

Our results describe the broad distribution of tiny HDV-like ribozymes. This finding builds on the previously shown prevalence of this fold throughout nature and indicates that the HDV ribozyme motif is a common tool for self-scission of RNA. The results indicate that the reduced structure of minimal HDV-like ribozymes is perhaps more susceptible to folding into diverse conformations stabilized by different divalent metal ion concentrations and identities, leading to unique kinetic profiles that differ significantly from canonical, and presumably more structured, HDV-like ribozymes.

■ ASSOCIATED CONTENT

Supporting Information

Figure S1. This material is available free of charge via the Internet at http://pubs.acs.org.

■ AUTHOR INFORMATION

Corresponding Author

*Phone: (949) 824-9132; E-mail: aluptak.uci.edu.

Funding

This work was supported by the Pew Charitable Trusts through the Pew Biomedical Scholars Program.

Notes

The authors declare no competing financial interest.

■ ACKNOWLEDGMENTS

We would like to thank Randi Jimenez for help with structure-based search methodologies, and Cassandra Burke for her invaluable help with experimental troubleshooting.

■ ABBREVIATIONS

HDV, Hepatitis Delta Virus; drz, delta-like ribozyme

■ REFERENCES

(1) Ferre-D'Amare, A. R., and Scott, W. G. (2010) Small self-cleaving ribozymes. *Cold Spring Harbor Perspect. Biol. 2*, a003574.

(2) Ferre-D'Amare, A. R., Zhou, K., and Doudna, J. A. (1998) Crystal structure of a hepatitis delta virus ribozyme. *Nature 395*, 567−574.

(3) Wadkins, T. S., Perrotta, A. T., Ferre-D'Amare, A. R., Doudna, J. A., and Been, M. D. (1999) A nested double pseudoknot is required for self-cleavage activity of both the genomic and antigenomic hepatitis delta virus ribozymes. *RNA 5*, 720−727.

(4) Ke, A., Zhou, K., Ding, F., Cate, J. H., and Doudna, J. A. (2004) A conformational switch controls hepatitis delta virus ribozyme catalysis. *Nature 429*, 201−205.

(5) Chen, J. H., Yajima, R., Chadalavada, D. M., Chase, E., Bevilacqua, P. C., and Golden, B. L. (2010) A 1.9 A crystal structure of the HDV ribozyme precleavage suggests both Lewis acid and general acid mechanisms contribute to phosphodiester cleavage. *Biochemistry 49*, 6508−6518.

(6) Das, S. R., and Piccirilli, J. A. (2005) General acid catalysis by the hepatitis delta virus ribozyme. *Nat. Chem. Biol. 1*, 45−52.

(7) Golden, B. L. (2011) Two distinct catalytic strategies in the hepatitis delta virus ribozyme cleavage reaction. *Biochemistry 50*, 9424−9433.

(8) Nakano, S., Chadalavada, D. M., and Bevilacqua, P. C. (2000) General acid-base catalysis in the mechanism of a hepatitis delta virus ribozyme. *Science 287*, 1493−1497.

(9) Fauzi, H., Kawakami, J., Nishikawa, F., and Nishikawa, S. (1997) Analysis of the cleavage reaction of a *trans*-acting human hepatitis delta virus ribozyme. *Nucleic Acids Res. 25*, 3124−3130.
(10) Cerrone-Szakal, A. L., Chadalavada, D. M., Golden, B. L., and Bevilacqua, P. C. (2008) Mechanistic characterization of the HDV genomic ribozyme: the cleavage site base pair plays a structural role in facilitating catalysis. *RNA 14*, 1746−1760.
(11) Chen, J. H., Gong, B., Bevilacqua, P. C., Carey, P. R., and Golden, B. L. (2009) A catalytic metal ion interacts with the cleavage Site G.U wobble in the HDV ribozyme. *Biochemistry 48*, 1498−1507.
(12) Sefcikova, J., Krasovska, M. V., Sponer, J., and Walter, N. G. (2007) The genomic HDV ribozyme utilizes a previously unnoticed U-turn motif to accomplish fast site-specific catalysis. *Nucleic Acids Res. 35*, 1933−1946.
(13) Thaplyal, P., Ganguly, A., Golden, B. L., Hammes-Schiffer, S., and Bevilacqua, P. C. (2013) Thio effects and an unconventional metal ion rescue in the genomic hepatitis delta virus ribozyme. *Biochemistry 52*, 6499−6514.
(14) Nishikawa, F., Fauzi, H., and Nishikawa, S. (1997) Detailed analysis of base preferences at the cleavage site of a trans-acting HDV ribozyme: a mutation that changes cleavage site specificity. *Nucleic Acids Res. 25*, 1605−1610.
(15) Perrotta, A. T., and Been, M. D. (2007) A single nucleotide linked to a switch in metal ion reactivity preference in the HDV ribozymes. *Biochemistry 46*, 5124−5130.
(16) Webb, C. H., Riccitelli, N. J., Ruminski, D. J., and Lupták, A. (2009) Widespread occurrence of self-cleaving ribozymes. *Science 326*, 953.
(17) Salehi-Ashtiani, K., Lupták, A., Litovchick, A., and Szostak, J. W. (2006) A genomewide search for ribozymes reveals an HDV-like sequence in the human CPEB3 gene. *Science 313*, 1788−1792.
(18) Webb, C. H., and Lupták, A. (2011) HDV-like self-cleaving ribozymes. *RNA Biol. 8*, 719−727.
(19) Wu, H. N., Lee, J. Y., Huang, H. W., Huang, Y. S., and Hsueh, T. G. (1993) Mutagenesis analysis of a hepatitis delta virus genomic ribozyme. *Nucleic Acids Res. 21*, 4193−4199.
(20) Tanner, N. K., Schaff, S., Thill, G., Petit-Koskas, E., Crain-Denoyelle, A. M., and Westhof, E. (1994) A three-dimensional model of hepatitis delta virus ribozyme based on biochemical and mutational analyses. *Curr. Biol. 4*, 488−498.
(21) Fauzi, H., Chiba, A., Nishikawa, F., Roy, M., Kawakami, J., and Nishikawa, S. (1998) Minimization of genomic human hepatitis delta virus ribozyme. *Anal. Chim. Acta 365*, 309−317.
(22) Li, L. L., Victoria, J., Kapoor, A., Blinkova, O., Wang, C. L., Babrzadeh, F., Mason, C. J., Pandey, P., Triki, H., Bahri, O., Oderinde, B. S., Baba, M. M., Bukbuk, D. N., Besser, J. M., Bartkus, J. M., and Delwart, E. L. (2009) A novel picornavirus associated with gastroenteritis. *J. Virol. 83*, 12002−12006.
(23) Nehdi, A., and Perreault, J. P. (2006) Unbiased in vitro selection reveals the unique character of the self-cleaving antigenomic HDV RNA sequence. *Nucleic Acids Res. 34*, 584−592.
(24) Legiewicz, M., Wichlacz, A., Brzezicha, B., and Ciesiolka, J. (2006) Antigenomic delta ribozyme variants with mutations in the catalytic core obtained by the in vitro selection method. *Nucleic Acids Res. 34*, 1270−1280.
(25) Riccitelli, N. J., and Lupták, A. (2010) Computational discovery of folded RNA domains in genomes and in vitro selected libraries. *Methods 52*, 133−140.
(26) Eickbush, D. G., and Eickbush, T. H. (2010) R2 retrotransposons encode a self-cleaving ribozyme for processing from an rRNA cotranscript. *Mol. Cell. Biol. 30*, 3142−3150.
(27) Ruminski, D. J., Webb, C. H., Riccitelli, N. J., and Lupták, A. (2011) Processing and translation initiation of non-long terminal repeat retrotransposons by hepatitis delta virus (HDV)-like self-cleaving ribozymes. *J. Biol. Chem. 286*, 41286−41295.
(28) Sanchez-Luque, F. J., Lopez, M. C., Macias, F., Alonso, C., and Thomas, M. C. (2011) Identification of an hepatitis delta virus-like ribozyme at the mRNA 5′-end of the L1Tc retrotransposon from Trypanosoma cruzi. *Nucleic Acids Res. 39*, 8065−8077.
(29) Victoria, J. G., Kapoor, A., Li, L., Blinkova, O., Slikas, B., Wang, C., Naeem, A., Zaidi, S., and Delwart, E. (2009) Metagenomic analyses of viruses in stool samples from children with acute flaccid paralysis. *J. Virol. 83*, 4642−4651.
(30) Blinkova, O., Rosario, K., Li, L., Kapoor, A., Slikas, B., Bernardin, F., Breitbart, M., and Delwart, E. (2009) Frequent detection of highly diverse variants of cardiovirus, cosavirus, bocavirus, and circovirus in sewage samples collected in the United States. *J. Clin. Microbiol. 47*, 3507−3513.
(31) Jimenez, R. M., Delwart, E., and Lupták, A. (2011) Structure-based search reveals hammerhead ribozymes in the human microbiome. *J. Biol. Chem. 286*, 7737−7743.
(32) Kurokawa, K., Itoh, T., Kuwahara, T., Oshima, K., Toh, H., Toyoda, A., Takami, H., Morita, H., Sharma, V. K., Srivastava, T. P., Taylor, T. D., Noguchi, H., Mori, H., Ogura, Y., Ehrlich, D. S., Itoh, K., Takagi, T., Sakaki, Y., Hayashi, T., and Hattori, M. (2007) Comparative metagenomics revealed commonly enriched gene sets in human gut microbiomes. *DNA Res. 14*, 169−181.
(33) Nakano, S., Proctor, D. J., and Bevilacqua, P. C. (2001) Mechanistic characterization of the HDV genomic ribozyme: assessing the catalytic and structural contributions of divalent metal ions within a multichannel reaction mechanism. *Biochemistry 40*, 12022−12038.
(34) Gong, B., Chen, J. H., Chase, E., Chadalavada, D. M., Yajima, R., Golden, B. L., Bevilacqua, P. C., and Carey, P. R. (2007) Direct measurement of a pK(a) near neutrality for the catalytic cytosine in the genomic HDV ribozyme using Raman crystallography. *J. Am. Chem. Soc. 129*, 13335−13342.
(35) Pontius, B. W., Lott, W. B., and vonHippel, P. H. (1997) Observations on catalysis by hammerhead ribozymes are consistent with a two-divalent-metal-ion mechanism. *Proc. Natl. Acad. Sci. U. S. A. 94*, 2290−2294.
(36) Nakano, S., Cerrone, A. L., and Bevilacqua, P. C. (2003) Mechanistic characterization of the HDV genomic ribozyme: classifying the catalytic and structural metal ion sites within a multichannel reaction mechanism. *Biochemistry 42*, 2982−2994.
(37) Ryder, S. P., and Strobel, S. A. (1999) Nucleotide analog interference mapping. *Methods 18*, 38−50.
(38) Prabhu, N. S., Dinter-Gottlieb, G., and Gottlieb, P. A. (1997) Single substitutions of phosphorothioates in the HDV ribozyme G73 define regions necessary for optimal self-cleaving activity. *Nucleic Acids Res. 25*, 5119−5124.
(39) Soukup, G. A., and Breaker, R. R. (1999) Relationship between internucleotide linkage geometry and the stability of RNA. *RNA 5*, 1308−1325.
(40) Harris, D. A., and Walter, N. G. (2003) Probing RNA structure and metal-binding sites using terbium(III) footprinting, *Curr. Protoc. Nucleic Acid Chem.*, Chapter 6, Unit 6.8.
(41) Suh, Y. A., Kumar, P. K., Taira, K., and Nishikawa, S. (1993) Self-cleavage activity of the genomic HDV ribozyme in the presence of various divalent metal ions. *Nucleic Acids Res. 21*, 3277−3280.
(42) Dominguez, D. C. (2004) Calcium signalling in bacteria. *Mol. Microbiol. 54*, 291−297.